JOURNAL OF CATALYSIS 149, 428–437 (1994)

Hydrogen and CO Intrapellet Diffusion Effects in Ruthenium-Catalyzed Hydrocarbon Synthesis

Rostam J. Madon[1] and Enrique Iglesia[2]

Corporate Research Laboratories, Exxon Research and Engineering Co., Annandale, New Jersey 08801

Received February 25, 1994; revised June 10, 1994

Intrapellet H_2 and CO concentration gradients within catalyst pellets during Fischer–Tropsch (FT) synthesis lead to lighter and more paraffinic hydrocarbon products than when intrapellet diffusion limitations are negligible. These transport restrictions decrease both H_2 and CO concentrations near catalytic sites and lead to significant changes in product selectivity. Time-on-stream experiments show that after an experiment is started methane and paraffin/olefin ratios increase rapidly while CO conversion and C_5+ selectivity decrease on diffusion-limited pellets until steady state is reached. These changes are not observed on pellets free from transport limitations. Our results indicate that CO concentrations decrease continuously and to a greater extent than H_2 concentrations from the exterior to the center of large liquid-filled pellets. Extreme intrapellet diffusion restrictions totally deplete CO near the pellet center and restore the hydrogenolysis activity of Ru which is otherwise strongly inhibited by CO during FT synthesis. In the absence of CO, large hydrocarbons that are removed slowly from liquid-filled catalyst pores undergo extensive hydrogenolysis on Ru sites close to or at the center of the pellets, leading to lower wax yields and to higher methane and light paraffin selectivity.

© 1994 Academic Press, Inc.

INTRODUCTION

In complex catalytic processes, intrapellet diffusion limitations of reactants and products often influence reaction rates and selectivities (1). The Fischer–Tropsch (FT) synthesis is a network of parallel and consecutive reactions that take place within catalyst pores filled with waxy liquid hydrocarbon product (2). As a result, severe intrapellet diffusion restrictions during FT synthesis that introduce H_2 and CO concentration gradients not only decrease reactant conversion rates, but also lead to product distributions that differ significantly from those formed under gradientless conditions. Shultz *et al.* (3) and Anderson and Hofer (4) first showed that intrapellet diffusion influenced FT synthesis reactions on large Fe-based catalyst pellets and that the reaction occurred predominantly on regions located within 0.1–0.4 mm of the outer pellet surface. Madon *et al.* (5) later confirmed these findings using the Prater–Weisz criterion (6) and suggested general requirements to avoid transport restrictions in FT synthesis. Recent studies on Fe (7) and Co (8, 9) catalysts have discussed reactant diffusion effects on FT synthesis rates but without describing their effect on selectivity.

Fischer–Tropsch synthesis rates are often assumed to be proportional to H_2 concentration (8, 9) and independent of CO concentration; such assumptions have led to simple models that conclude H_2 to be the diffusion-limited reactant while neglecting the effect of CO concentration gradients (7–9). Fischer–Tropsch synthesis kinetics are in reality described by Langmuir–Hinshelwood kinetic expressions (10–12), which become negative order in CO at experimental conditions of interest. These kinetic expressions are specific to each hydrocarbon product, and CO kinetic orders tend to become increasingly negative for lighter products (10). As a result, any decrease in CO concentration selectively favors the formation of lighter FT synthesis products. Recent experimental results and quantitative treatments of intrapellet diffusion on Co catalysts (11, 12) confirm the intuitive conclusion that the larger reactant (CO) exhibits the more severe intrapellet concentration gradients and is the diffusion limited reactant.

In addition to slowing down the arrival of reactants at catalytic sites, intrapellet diffusion also influences the removal rate and secondary reactions of reactive FT synthesis products, such as α-olefins, and significantly modifies the product molecular weight and functionality. Recently, we described the *diffusion-enhanced olefin readsorption* model (2, 11–15) which explains the non-Flory hydrocarbon product distributions usually obtained in FT synthesis. Removal of product α-olefins from catalyst pores becomes increasingly difficult because intrapellet diffusion rates decrease as α-olefin size increases; this leads to longer pellet residence times, higher readsorption probabilities, and heavier and more paraffinic products.

[1] Current address: Engelhard Corp., 101 Wood Avenue, Iselin, NJ 08830.

[2] Current address: Department of Chemical Engineering, University of California at Berkeley, Berkeley, CA 94720.

0021-9517/94 $6.00
Copyright © 1994 by Academic Press, Inc.
All rights of reproduction in any form reserved.

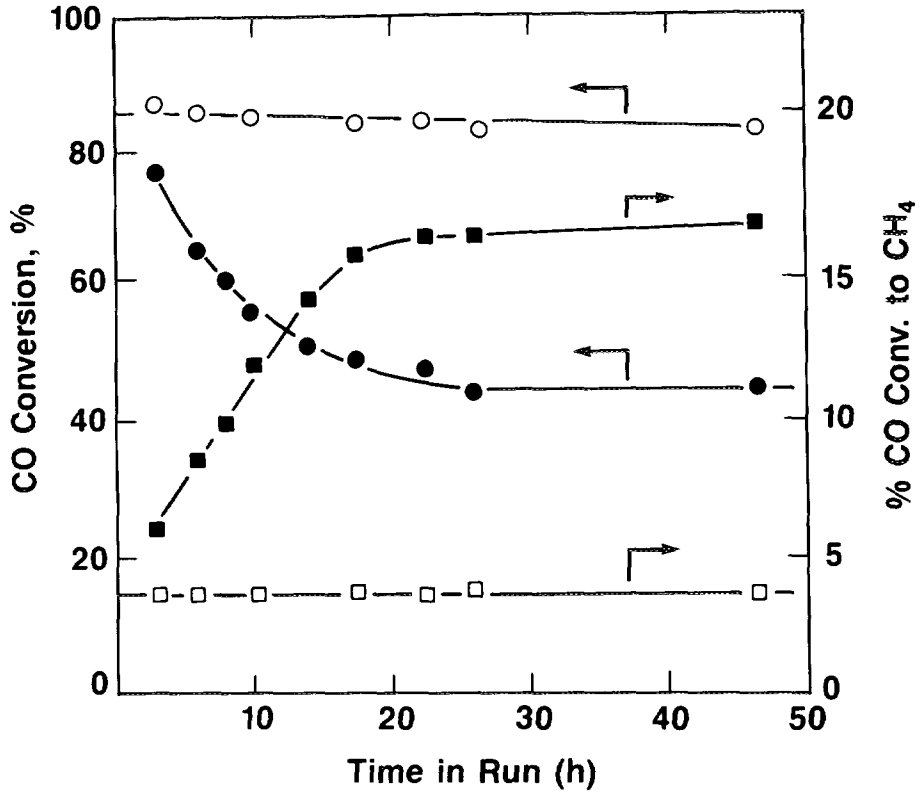

FIG. 1. CO conversion and methane selectivity with time in run (1% Ru/TiO_2, 489 K, 505 kPa, $H_2/CO = 2.00 \pm 0.03$). Closed symbols, large pellets (0.85–1.7 mm); open symbols, small pellets (0.11–0.18 mm).

In Refs. (2, 11–15), we focused on the role of intrapellet diffusion limitations of α-olefins on FT synthesis selectivity for Ru, Co, and Fe-based catalysts, while describing the corresponding reactant diffusion models for Co-based catalysts (11, 12). Here, we describe the influence of reactant diffusion on Ru catalysts, discuss the effect of CO and H_2 intrapellet concentration gradients on product selectivity, and suggest an experimental criterion to detect the presence of such intrapellet concentration gradients. Finally, we show how the intrinsic hydrogenolysis activity of Ru introduces additional complexity into any rigorous description of FT synthesis selectivity, and propose how to exploit these intrapellet diffusion restrictions to design catalysts with significantly lower yields of $C_{20}+$ hydrocarbons.

EXPERIMENTAL

Our experimental studies were carried out in a reactor system consisting of seven stainless steel packed-bed tubular reactors —1.22 m long and 0.77 cm internal diameter, embedded within a heated copper block (16). This system allowed direct comparisons between large and small catalyst pellets at identical temperature, pressure, H_2/CO ratio, and time on stream, while permitting independent changes in flow and space velocity required to maintain similar reactant conversion levels in all reactors. A controlled three-zone heater within the copper block, and the small diameter of the reactor ensured uniform bed temperatures as confirmed by a traveling thermocouple contained within a thermowell along the reactor center. Carbon monoxide, H_2, CO_2, and C_5- hydrocarbons were analyzed by on-line gas chromatography. Condensed C_5+ products were collected for 24 h after reaching steady state at a given set of reaction conditions and analyzed by gas and gel-permeation chromatography using procedures previously described (2).

In order to investigate intrapellet diffusion effects on Ru-catalyzed FT synthesis, we used Ru/TiO_2 catalysts of two pellet sizes. First, we prepared a 1 wt% Ru/TiO_2 on 0.85–1.7 mm (12–20 mesh) TiO_2 pellets using Degussa P-25 TiO_2 and $Ru(NO_3)_3$ solutions (Engelhard) (2). The surface area of TiO_2 was 40 m^2g^{-1} with an average pore size of 28 nm. Energy dispersive (EDAX) analysis in a scanning electron microscope showed that Ru was uniformly distributed throughout the pellets. This catalyst was reduced in flowing H_2 at 723 K for 4 h and passivated

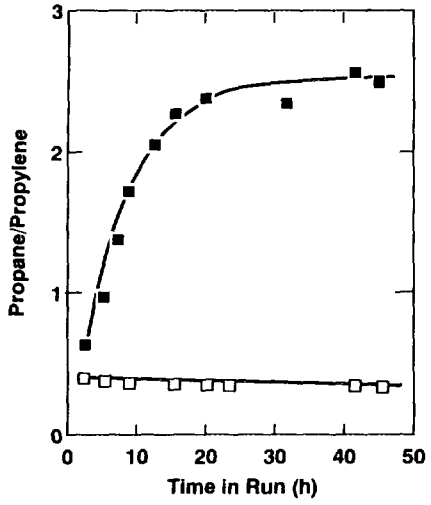

FIG. 2. Propane/propylene ratio with time in run (1% Ru/TiO_2, 489 K, 505 kPa, H_2/CO = 2.00 ± 0.03). Closed symbols, large pellets [0.85–1.7 mm]; open symbols, small pellets [0.11–0.18 mm].

at room temperature using dilute O_2. A portion of this sample was crushed and sieved to retain 0.11–0.18 mm (80–140 mesh) pellets. This procedure ensured that all catalyst parameters, such as metal loading, dispersion, support pore structure, and purity were identical and that only the characteristic diffusion path length differed between these two samples. The average Ru crystallite size measured by transmission electron microscopy after FT synthesis was 2.0–2.5 nm for the 1.0 wt% Ru/TiO_2 catalyst. Another catalyst, 0.97 wt% Ru/TiO_2, was prepared using small 0.11–0.18 mm TiO_2 pellets and a procedure identical to that described above. All catalysts after being loaded into the reactor were reduced again in flowing H_2 for 4 h at 673 K and purged with Ar before synthesis gas was introduced.

RESULTS

Fischer–Tropsch synthesis conversion rates and selectivity data on large and small 1% Ru/TiO_2 pellets are compared in Figs. 1–3 for experiments carried out simultaneously in our multiple reactor unit at 2.0 inlet H_2/CO ratio, 489 K, and 5 bar total pressure. Selectivities are reported as the percentage of converted CO appearing as a given hydrocarbon product. The earliest reported data were obtained after 2.5 h on stream, and the experiments lasted 240 h. Carbon monoxide conversion within the large pellets decreased from 78 to 48% during the first 20 h on stream (Fig. 1). In contrast, CO conversion within small pellets decreased only slightly due to deactivation from the initial high value of 88 to 84% over the first 20 h on stream. Over the next 220 h on stream, both catalysts decreased slightly and by the same extent due to deactivation. At steady state, the site time yield was 3.1×10^{-2} s^{-1} for the small pellets (14) and 1.4×10^{-2} s^{-1} for the large pellets. On the latter, the decrease in conversion was accompanied by a marked increase in CH_4 selectivity which increased from 6 to 17% during the first 20 h and then stayed constant for the remaining 220 h of the experiment. On small pellets, CH_4 selectivity was much lower (3.6%) and remained constant throughout the entire experiment. The propane/propylene selectivity ratio (Fig. 2) also increased markedly from 0.6 to 2.5 during the first 20 h on large pellets and then remained constant. In contrast, this selectivity ratio decreased slightly from 0.39 to 0.32 on the smaller catalyst pellets. The C_5+ selectivity (Fig. 3) on large pellets decreased from 80 to 66% during the first 20 h and then remained constant. On small pellets, the selectivity actually increased slightly from 87.5 to 89.5% during the first 50 h. At steady state, the $C_{20}+$ fraction of the total hydrocarbon product was 2.5 times greater on the smaller catalyst pellets.

Previously (14), we showed that on small Ru catalyst pellets higher H_2/CO reactant ratios favored CH_4 formation and decreased the selectivity to high molecular weight products. These effects are more severe on larger pellets (Fig. 4) where $C_{41}+$ selectivity decreased more than tenfold, and the CH_4 selectivity increased by a factor of 7 as the H_2/CO ratio increased from 1.0 to 2.8. The corresponding selectivities on smaller pellets changed only by factors of 2.5 and 3.5, respectively.

Fischer–Tropsch synthesis product distributions are often described by the Flory equation for polymerization processes (17)

$$\ln \frac{W_n}{n} = \ln \frac{(1-\alpha)^2}{\alpha} + n \ln \alpha, \qquad [1]$$

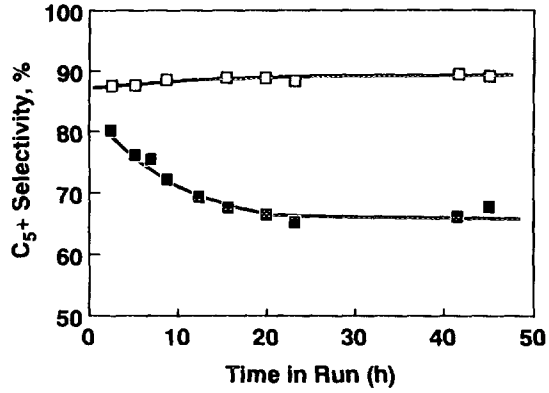

FIG. 3. C_5+ selectivity with time in run (1% Ru/TiO_2, 489 K, 505 kPa, H_2/CO = 2.00 ± 0.03). Closed symbols, large pellets [0.85–1.7 mm]; open symbols, small pellets [0.11–0.18 mm].

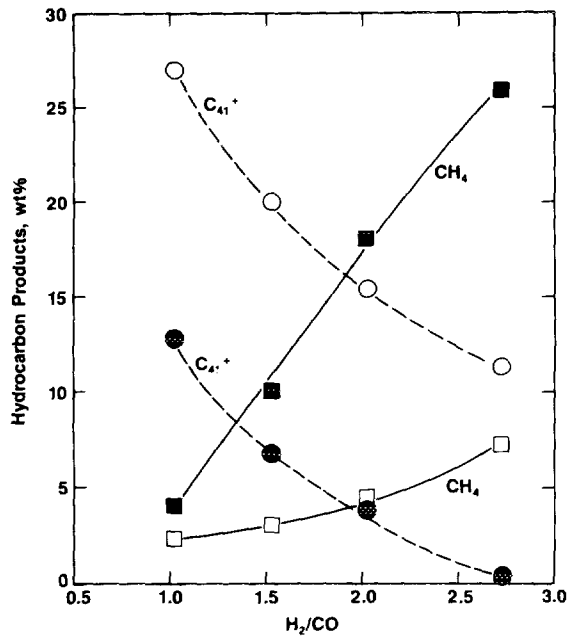

FIG. 4. CH_4 and C_{41}+ hydrocarbon selectivities with inlet H_2/CO ratios (1% Ru/TiO_2, 489 K, 505 kPa, $H_2/CO = 2.00 \pm 0.03$). Closed symbols, large pellets [0.85–1.7 mm]; open symbols, small pellets [0.11–0.18 mm].

where α is the growth probability of hydrocarbon chains,

$$\alpha = \frac{r_t}{r_t + r_p}. \qquad [2]$$

W_n is the selectivity (weight percent) of products with n carbons, and the chain growth parameter, α, relates the rates of chain propagation (r_p) and termination (r_t). A linear plot of ln W_n/n versus n indicates that α is independent of chain size and the chain growth process obeys Flory kinetics (17). Flory kinetics, however, seldom describe experimental FT synthesis product distributions at conditions favoring chain growth (2, 11–15). At such conditions, Flory plots are frequently curved because diffusion-enhanced α-olefin readsorption and chain initiation lead to an increase in α with increasing chain size (2, 11–15). The chain growth probability becomes independent of n only after olefins are totally consumed (e.g., for C_{35}+ products); Flory plots then become linear because longer pellet residence times cannot increase α further. Product distribution plots for large and small pellets at inlet H_2/CO ratios of 1, 2, and 3.2 are shown in Figs. 5–7.

Figure 5 shows carbon number distributions for large and small pellets at a reactant H_2/CO ratio of 1.0; CO conversions with the small and large pellets are similar with values of 25 and 19%, respectively. Lighter products are formed on the larger pellets; the C_{21}+ selectivity is 32%, compared to 48% on the smaller pellets. On both catalysts, Flory plots are curved, reflecting a strong influence of diffusion-enhanced olefin readsorption and chain initiation on both small and large pellets at reactant H_2/CO ratios near 1. Synthesis products are more paraffinic on large pellets; the propane/propylene and ethane/ethylene selectivity ratios on large pellets, are 0.34 and 1.5, respectively, and 0.25 and 0.9 on the smaller pellets.

Figures 6 and 7 show carbon number distributions obtained when the inlet H_2/CO ratio was switched from 2.0 to 3.2. First, the catalysts were exposed to synthesis gas with a H_2/CO ratio of 2 for 380 h and steady-state carbon number distributions measured on both small and large pellets (Fig. 6) at CO conversions of 78 and 72%, respectively. Carbon number differences between large and small pellets become greater at higher H_2/CO ratios (cf. Figs. 5 and 6). At a H_2/CO ratio of 2.0, the C_{21}+ product selectivity on large pellets is only 17 wt%, compared with 40 wt% on smaller pellets. After reaction for 380 h with an inlet H_2/CO ratio of 2, this ratio was changed to 3.2 and the space velocity adjusted to maintain similar CO conversions, about 75%, on both large and small pellets. Neither the H_2 nor CO flow was stopped during this change in composition; experimental continuity was preserved to ensure that catalyst pores remained filled with the hydrocarbon liquid products made previously with a H_2/CO ratio of 2. Steady-state carbon number distributions are shown in Fig. 7 for a H_2/CO ratio of 3.2 after 170 h on stream at this reactant composition. On small pellets, the Flory plot shows the usual curvature and the expected increase in chain growth probability with increasing chain size. However, the product distribution on the large pellets is significantly altered with a sharp drop in selectivity after C_{25}; no measurable amounts of C_{35}+ products were obtained. The results of Fig. 7 are at steady state and remained unchanged for 72 h at which time the experiment was ended. Product distributions on large and small pellets at H_2/CO ratios of 3.2 are also compared in Fig. 8. The C_{21}+ selectivity on large pellets is only 6% compared to 37% on smaller pellets. The C_5–C_{20} hydrocarbon selectivities are similar on both pellet sizes, but CH_4 and C_2–C_4 selectivities are much higher on the larger pellets. Products are predominantly paraffinic on large pellets as indicated by the propane/propylene ratio of 6.9 versus 0.45 on the small pellets.

Table 1 shows results on small pellets of 0.97 wt% Ru/TiO_2 at 481 K, 5 bar pressure, and a H_2/CO ratio of 3. At a gas hourly space velocity (GHSV) of 300 V/V.h (STP) and 85% CO conversion, CH_4 selectivity is 9.9% and C_5+ selectivity is 75%. When the space velocity is reduced to 150 V/V.h, CO is completely consumed. Carbon monoxide and olefins are no longer observed in the reactor effluent; CH_4 selectivity increases significantly to 18.5% at the expense of lower C_5+ selectivity.

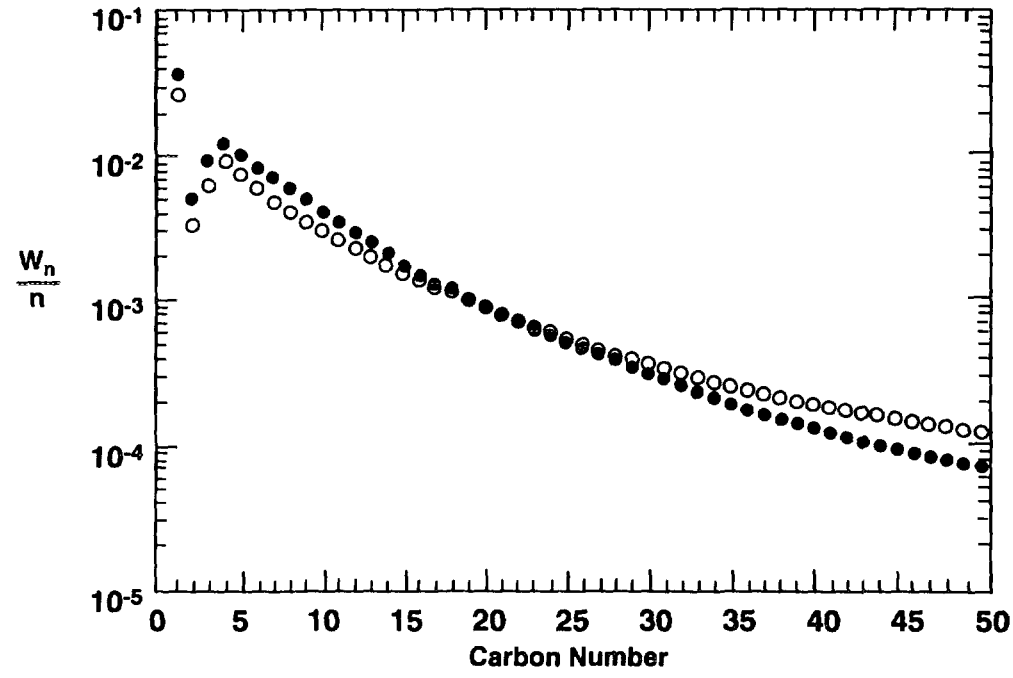

FIG. 5. Hydrocarbon product distributions (see Eq. [1]) at inlet H_2/CO ratio of 1.00 ± 0.03 (1% Ru/TiO_2, 489 K, 505 kPa). Closed symbols, large pellets [0.85–1.7 mm]; open symbols, small pellets [0.11–0.18 mm].

DISCUSSION

Fischer–Tropsch synthesis activity and selectivity on large pellets changes markedly during the first 20 h of reaction (Figs. 1–3). In contrast, synthesis rates and selectivities on small pellets are relatively unaffected by time on stream. On large pellets, CO conversion decreases and CH_4 selectivity increases with time on stream while the product distribution becomes lighter and more paraffinic. These changes occur in large pellets because H_2 and CO concentration gradients develop within catalyst pores as they become filled with hydrocarbon liquid products. At the start of the experiment, selectivities are identical on large and small pellets because neither pellet size imposes a diffusion restriction to reactant arrival in the absence of an intrapellet liquid phase. The data obtained after 2.5 h time on stream already show activity and selectivity differences between the pellets. As the reaction proceeds, intrapellet pores continue to fill with liquid products, and the differences between small and large pellets become greater until a steady state is reached at about 20 h on stream when all pores in the large pellets are filled with liquid. Pores within smaller pellets fill with liquid in less than 2.5 h at our conditions, but the intrapellet liquid phase does not introduce any significant diffusion restrictions because of the short diffusion path required to access intrapellet active sites. Pore filling times are also much shorter (<2.5 h) on small than on large pellets (~20 h) because of the higher FT synthesis rates and C_5+ yields obtained under kinetically controlled conditions on small pellets.

These data suggest a simple experimental criterion to detect the presence of intrapellet reactant diffusion effects in FT synthesis. *If methane selectivity and propane/propylene (or other paraffin/olefin) ratio increase, and C_5+ selectivity and CO conversion decrease, within the first several hours on stream, then the synthesis reaction is influenced by intrapellet concentration gradients of CO and H_2.* The magnitude of these changes in selectivity and activity will depend on the nature of the catalyst and on the experimental conditions, but the general trends will be observed irrespective of catalyst or reaction conditions when intrapellet diffusional restrictions occur.

Previously (14), we discussed the importance of H_2 and CO concentrations in determining FT synthesis selectivities on small pellets unaffected by intrapellet reactant diffusion. As H_2 concentration increases or CO concentration decreases in the liquid phase, the ratio of surface hydrogen (H*) to surface monomer ($*CH_2$) concentration increases, and chain termination to paraffins (r_h) is favored,

$$\frac{r_h}{r_o} = \frac{k_h}{k_o} \cdot \frac{(*C_n)(H*)}{(*C_n)} = \frac{k_h}{k_o} \cdot (H*), \qquad [3]$$

where r_o is the chain termination rate to olefins, k's are termination rate constants, and $*C_n$ is a surface hydrocar-

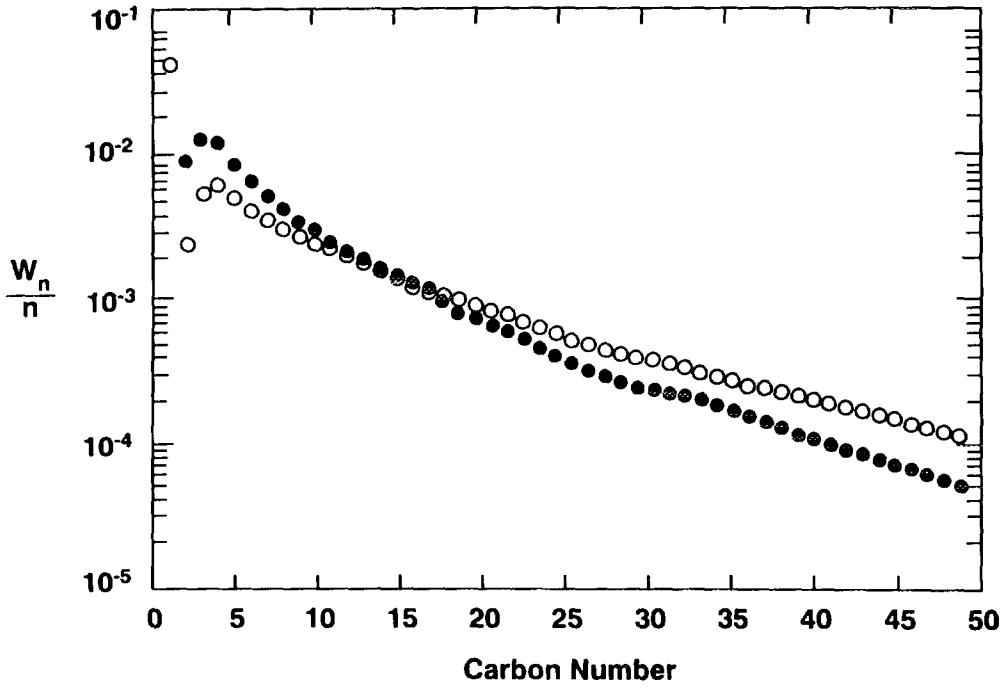

FIG. 6. Hydrocarbon product distributions (see Eq. [1]) at inlet H_2/CO ratio of 2.00 ± 0.03 (489 K, 505 kPa). Closed symbols, 1% Ru/TiO_2, large pellets [0.85–1.7 mm]; open symbols, 0.97% Ru/TiO_2, small pellets [0.11–0.18 mm].

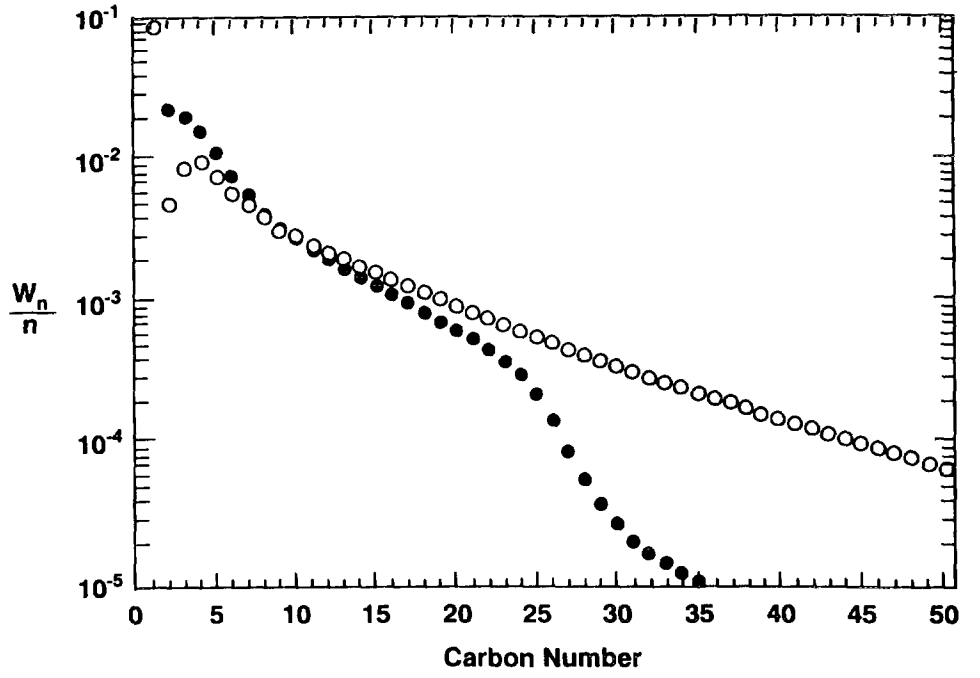

FIG. 7. Hydrocarbon product distributions (see Eq. [1]) at inlet H_2/CO ratio of 3.20 ± 0.03 (489 K, 505 kPa). Closed symbols, 1% Ru/TiO_2, large pellets [0.85–1.7 mm]; open symbols, 0.97% Ru/TiO_2, small pellets [0.11–0.18 mm].

TABLE 1

Effect of CO Depletion on FT Synthesis Selectivity (0.97% Ru/TiO_2, H_2/CO = 3.0, P = 5 bar, T = 481 K, Pellet Diameter = 0.11–0.18 mm)

	(V/V·h) Space velocity	
	300	150
CO conversion, (%)	85	100
H_2 conversion, (%)	60	74
CO concentration at reactor exit (mol%)	9	0
Selectivities		
CH_4	9.9	18.5
C_2H_6	1.5	2.8
C_2H_4	0.03	0
C_3H_8	2.8	5.3
C_3H_6	2.5	0
$N\text{-}C_4H_{10}$	3.7	6.4
$1\text{-}C_4H_8$	1.6	0
trans-$2\text{-}C_4H_8$	0.8	0
cis-$2\text{-}C_4H_8$	1.4	0
C_5+	75	67

bon chain with n carbons. Also, as H_2 concentration increases or CO concentration decreases, α-olefin readsorption rates decrease and the overall chain termination probability (β), defined as the ratio of chain termination to chain propagation rates, increases *for all carbon numbers* (14). Thus, FT synthesis products become lighter and more paraffinic as the concentration of CO (or more rigorously the fugacity) in the liquid phase decreases relative to that of H_2. In small pellets, when there are no reactant transport restrictions, as in Ref. (14), phase equilibrium ensures that liquid phase fugacities of H_2 and CO throughout the pellet are equal to their corresponding gas fugacities (pressures) outside the pellet. As a result, surface fugacities are constant throughout the pellet and directly reflect the gas phase interpellet partial pressures of H_2 and CO; at these conditions synthesis reactions are unaffected by the presence of intrapellet liquids.

In large pellets, with intrapellet diffusion restrictions, liquid phase fugacities of H_2 and CO within the pores are not equal to gas phase fugacities outside the pellet. Liquid phase fugacities, and hence concentrations, of H_2 and CO decrease continuously from the outer surface to the center of the pellets. Under our conditions, selectivity results suggest that CO liquid concentration decreases more rapidly along the pore than that of H_2. Thus the liquid phase concentration ratio of H_2/CO increases continuously as we move toward the center of the pellet. This decrease in CO liquid concentration relative to H_2 favors the formation of light paraffins because active sites become starved of CO precursors for the monomer ($*CH_2$) required in chain growth, while the relatively larger concentration of H* preferentially terminates surface chains as unreactive paraffins. Intrapellet diffusion restrictions increase the $(H^*)/(*CH_2)$ ratio continuously within the pores.

Since our small and large Ru/TiO_2 pellets are identical except for their pellet diameter, we can calculate catalyst effectiveness factors (η_L) for large pellets directly from measured FT synthesis reaction rates. Effectiveness factor (1), defined as the ratio of measured rates to the kinetic rates in the absence of intrapellet diffusion restrictions, is assumed to be 1 for the small pellets as shown by the results in Figs. 1–3. On large pellets, η_L values are 0.60, 0.52, and 0.46 for H_2/CO ratios of 1, 2, and 2.8, respectively. This trend reflects the fact that lower CO concentrations influence diffusion rates, which are proportional to CO concentration, more strongly than reaction rates which depend more weakly on CO concentration (14).

Intrapellet diffusion limitations may be described in terms of the Damköhler number (Da) of the second kind (6) which reflects the ratio of kinetic to diffusion rates within pellets of diameter d_p and is defined for CO or H_2 as

$$\mathrm{Da}_i = \frac{d_p^2 r_i}{C_{s,i} D_{e,i}}, \qquad [4]$$

where r_i is the reaction rate, $C_{s,i}$ the concentration in the hydrocarbon liquid at the pore mouth, and $D_{e,i}$ the effective diffusivity. We calculated diffusivities with the Wilke–Chang equation (18), used a porosity to tortuosity ratio of 0.2, and obtained concentrations by multiplying Henry's constants (4, 8, 19, 20) with the reactant partial pressure. We used kinetic rates (r_i) on small pellets free

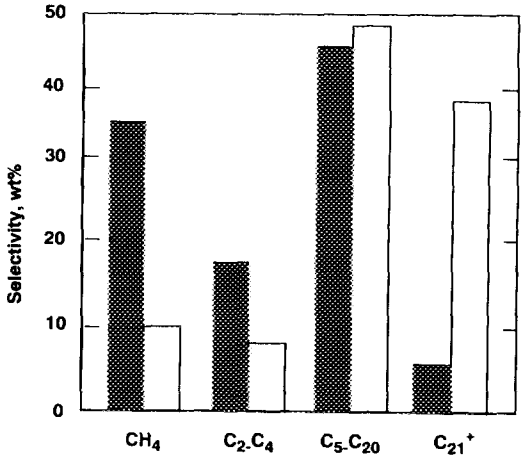

FIG. 8. Hydrocarbon selectivities from the data in Fig. 7. Black bars, 1% Ru/TiO_2, large pellets [0.85–1.7 mm]; white bars, 0.97% Ru/TiO_2, small pellets [0.11–0.18 mm].

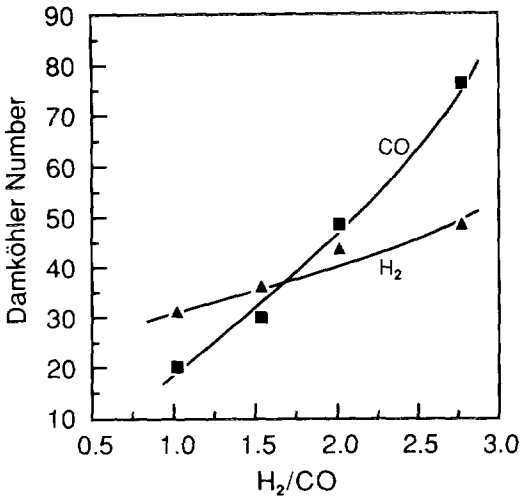

FIG. 9. Damköhler numbers for H_2 (triangles) and CO (squares) versus inlet H_2/CO ratio; 1% Ru/TiO_2, large pellets [0.85–1.7 mm].

from diffusion limitations, which would also be the rates at the exterior of the large pellets. Figure 9 shows Damköhler number plots for CO and H_2 on large pellets as a function of inlet H_2/CO ratio. All values for Da_{CO} and Da_H are significantly greater than 1, thus indicating (6) that reactions of CO and H_2 are transport limited on pellets of about 1 mm diameter at our conditions. Carbon monoxide is the reactant with the more marked intrapellet concentration gradients at higher H_2/CO ratios. The trends in Fig. 9 are consistent with severe diffusional limitations that occur as CO concentration decreases (H_2/CO ratio increases); diffusion rates decrease proportionately as CO concentration decreases while kinetic consumption rates may actually increase due to the negative order CO kinetics of the FT reaction (10). However, at all H_2/CO ratios investigated, product selectivity on intrapellet diffusion-limited pellets is determined by low CO concentrations; we have never observed an increase in product molecular weight under such diffusion-limited conditions.

Even for H_2/CO reactant ratios as low as 1, hydrocarbon distributions shown in Fig. 5 suggest that lighter products form preferentially on larger pellets. The plots for small and large pellets intersect at about C_{20} and resemble those previously reported (14) for synthesis products on small pellets at reactant ratios of 1 and 2.8. This is not surprising because CO concentration gradients within large pellets lead to lower CO concentrations within intrapellet liquids and to liquid phase H_2/CO concentration ratios greater than 1.0 near active sites. As a result, chain termination probabilities (β_n) are greater on large pellets for every chain size C_n resulting in lower molecular weight FT synthesis products.

Differences in product molecular weight and paraffin content between small and large pellets become more pronounced for H_2/CO reactant ratios of 2 (Fig. 6), and the plots for the two pellet sizes intersect at about C_{10}. This greater sensitivity to pellet diameter reflects more severe diffusion restrictions and concentration gradients as (a) the kinetic load is increased due to the higher intrinsic kinetic rates at higher H_2/CO ratios, and (b) CO diffusion rates are lower as CO concentration decreases. At all synthesis gas compositions, Flory distribution plots are curved and diffusion-enhanced α-olefin readsorption (2, 11–15) plays a critical role in modifying chain growth pathways and FT synthesis selectivity on both large and small pellets. The effectiveness of these α-olefin readsorption and chain initiation pathways, however, is less on larger pellets, where higher H_2/CO concentration ratios in the liquid favor desorption as unreactive paraffins. Similar effects were reported previously (14) as the inlet H_2/CO ratio increased on small catalyst pellets.

When the inlet H_2/CO ratio is switched from 2 to 3.2, the hydrocarbon product distribution on large pellets changes dramatically (Fig. 7). Selectivity changes are observed within 24 h of the reactant composition change; CH_4 selectivity increases from 11 to 30%, and selectivity to C_5+ chains decreases from 76 to 52%. These selectivity values are constant for the remaining 192 h of the experiment. A decrease in C_{25}+ selectivity occurs after the initial 24 h as condensed hydrocarbons formed at a H_2/CO ratio of 2 are removed slowly from the reactor. As they are removed, a new vapor–liquid equilibrium is established, and the product distribution changes monotonically between that in Fig. 6, for H_2/CO = 2, to that in Fig. 7, for H_2/CO = 3.2. Results shown in Figs. 7 and 8 were obtained after steady state was reached in the liquid phase 144 h after the reactant ratio switch; these results remained unchanged for an additional 72 h, at which time the experiment was ended. Steady-state distributions very similar to those in Fig. 7 were also obtained when a separate experiment was carried out for 168 h on the large pellets at only one H_2/CO ratio of 2.8, i.e., without any inlet reactant composition change. Thus the same steady-state results are obtained when large pellets are either empty or filled with hydrocarbon liquid at the start of an experiment with H_2/CO ratio of 2.8–3.2. The marked drop in C_{25}+ selectivity at high reactant ratios is quite unusual and was not observed on pellets that are free from intrapellet CO and H_2 diffusion limitations. Clearly the sharp break in an otherwise monotonic carbon number distribution is due to chemistry other than the normal stochastic polymerization processes modified by olefin readsorption and chain initiation.

As inlet H_2/CO ratios become greater than 2.0, severe intrapellet reactant concentration gradients occur within large pellets. Since CO reaction rates actually increase with decreasing CO concentration and increasing H_2/CO ratio (14), at some pellet radial position all CO is totally

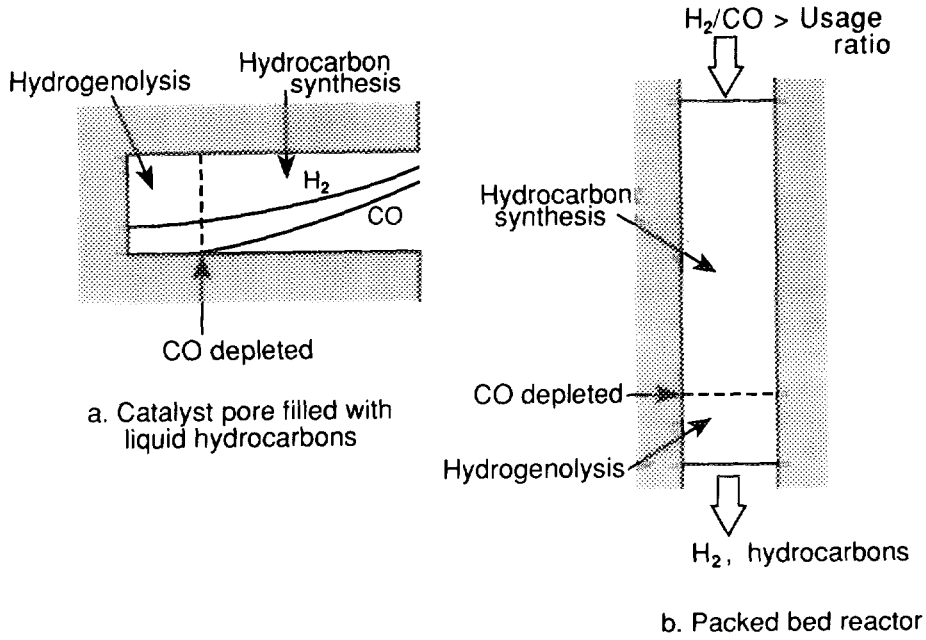

FIG. 10. Hydrogenolysis takes place on Ru (a) within catalyst pores or (b) in the reactor, when CO is completely depleted.

depleted from intrapellet liquids, and the region of the pellet near its center contains only hydrocarbon products and unreacted H_2. In the absence of CO, paraffins readily undergo hydrogenolysis on Ru at normal FT synthesis temperatures. Larger molecules, with longer pellet residence times and larger number of reactive C–C bonds, undergo hydrogenolysis preferentially over faster diffusing and less reactive smaller paraffins. Our results (Figs. 7 and 8) show that C_{35}+ hydrocarbons do not leave the pellet when CO is totally depleted within the pellet.

The substantial decrease in C_{21}+ hydrocarbons on large pellets is balanced by an increased selectivity to C_1–C_4 hydrocarbons (Fig. 8). Paraffin hydrogenolysis on Ru, unlike on Ni, does not take place solely at terminal C–C bonds (21), although recent results (22) with hexadecane show that terminal cracking is preferred over midmolecule cracking. The large increase in the selectivity to C_1–C_4 products may be the result of multiple cracking events or of steric forces that favor hydrogenolysis at or near the end of large chains in the waxy hydrocarbon environment within the pores.

In the absence of CO, paraffin hydrogenolysis should occur not only within Ru-based catalyst pellets but also as CO is totally consumed along the catalyst bed. At very low space velocities, CO can be totally depleted near the exit region of tubular reactors. Table 1 shows data obtained when this occurs within a bed of small Ru/TiO_2 pellets at a H_2/CO reactant ratio (3.0) greater than the stoichiometric consumption ratio (~2.05), conditions that guarantee that CO can be totally consumed. In this experiment, since only small catalyst pellets are used, there are no intrapellet reactant diffusion effects, and the complete consumption of CO before the exit of the catalyst bed is due to the low space velocity used. At 300 V/V.h, we observe typical product selectivities, but when the space velocity is decreased further to 150 V/V.h, CO is completely consumed before the reactor outlet. Hydrocarbons are synthesized near the inlet of the reactor, where CO precursors to the required monomers are abundant, but undergo hydrogenolysis and hydrogenation reactions near the CO-starved reactor outlet. Methane selectivity increases significantly, suggesting multiple hydrogenolysis events and preferential terminal cracking. These bed effect results confirm our proposal that intrapellet CO depletion accounts for the unusual carbon number distributions reported in Figs. 7 and 8. Figure 10 depicts CO depletion and hydrogenolysis regions within a pellet and a catalyst bed.

These effects of bed and intrapellet CO depletion on hydrogenolysis rates were not observed on Co catalysts (11, 12) where paraffin hydrogenolysis is slower than on Ru even in the absence of CO. Hexane hydrogenolysis rates (21) on Ru are two orders of magnitude greater than on Co. A recent study (22) using hexadecane showed hydrogenolysis turnover rates on Ru catalysts to be about 10 times greater than on Co at typical FT synthesis temperatures and H_2 pressures.

Differences in selectivity between identical catalysts operated in gas phase and three-phase (slurry) reactors

have been incorrectly attributed to solubility-enhanced hydrogenolysis of large paraffins (23). A proposal (23) that the higher solubility of large hydrocarbons within FT synthesis liquids increases their pore residence time cannot account for the higher probability of forming light hydrocarbons in three-phase reactors. In the absence of transport restrictions, gas and liquid phase remain at equilibrium and the reactant and product fugacities in the liquid phase are identical to those in the gas phase and independent of the solubility properties of the hydrocarbon molecules and of the chemical identity of the liquid phase. Solubility of a molecule by itself cannot influence the kinetic driving force for its secondary reactions (11, 14). The reported selectivity changes must reflect instead diffusion limitations of reactants within liquid-filled catalyst pores; these diffusional restrictions lower CO concentrations and increase H_2/CO ratios within intrapellet liquids leading to the observed higher selectivities to light products.

Lafayatis and Foley (24) simulated the effects of diffusion-enhanced hydrogenolysis during FT synthesis by modeling catalyst pellets with carbon coatings which could preferentially retain larger hydrocarbons. In this scheme, secondary hydrogenolysis reactions could increase selectivity to light products if intrapellet sites catalyzed such reactions in the presence of CO and H_2O at FT synthesis temperatures. This is difficult to accomplish in practice because of the strong inhibition of C–C bond cleavage steps on both metal and acid sites by CO and water. However, we can obtain substantially higher yields of lighter product, which do not obey conventional Flory distributions, when severe intrapellet reactant transport limitations deplete CO near hydrogenolysis sites placed near the pellet center (Figs. 7 and 8). Additional benefits would be obtained by designing intrapellet sites that favor midmolecule C–C bond cleavage instead of terminal hydrogenolysis typical of most metal catalysts. Acid sites favor midmolecule cracking and can also be used to exploit the selective retention of large molecules within catalyst pellets, as shown previously by detailed mathematical simulations of FT synthesis selectivities on bifunctional metal–acid catalysts (11, 12, 25).

REFERENCES

1. Wheeler, A., *Adv. Catal. Relat. Subj.* **3,** 249 (1951).
2. Madon, R. J., Reyes, S. C., and Iglesia, E., *J. Phys. Chem.* **95,** 7795 (1991).
3. Shultz, J. F., Abelson, M., Stein, K. C., and Anderson, R. B., *J. Phys. Chem.* **63,** 496 (1959).
4. Anderson, R. B., and Hofer, L. J. E., *J. Chem. Eng. Data* **5,** 511 (1960).
5. Madon, R. J., Bucker, E. R., and Taylor, W. F., Dept. of Energy, Final Report, Contract No. E (46-1)-8008, July 1977.
6. Weisz, P. B., and Prater, C. D., *Adv. Catal. Relat. Subj.* **6,** 143, (1954); Weisz, P. B., *Z. Phys. Chem. Neue Folge* **11,** 1 (1957).
7. Zimmerman, W. H., Rossin, J. A., and Bukur, D. B., *Ind. Eng. Chem. Res.* **28,** 406 (1989).
8. Post, M. F. M., van't Hoog, A. C., Minderhoud, J. K., and Sie, S. T., *AIChE Journal* **35,** 1107, (1989).
9. Sie, S. T., Senden, M. M. G., and van Wechem, H. M. H., *Catal. Today* **8,** 371 (1991).
10. Kellner, C. S., and Bell, A. T., *J. Catal.* **70,** 418 (1981).
11. Iglesia, E., Reyes, S. C., Madon, R. J., and Soled, S. L., *Adv. Catal. Relat. Subj.* **39,** 221 (1993).
12. Iglesia, E., Reyes, S. C., and Soled, S. L., *in* "Computer Aided Design of Catalysts and Reactors" (R. E. Becker, and C. J. Pereira, Eds.) Dekker, New York, 1993.
13. Iglesia, E., Reyes, S. C., and Madon,R. J., *J. Catal.* **129,** 238 (1991).
14. Madon, R. J., and Iglesia, E., *J.Catal.* **139,** 576 (1993).
15. Madon, R. J., Iglesia, E., and Reyes, S. C., *in* "Selectivity in Catalysis" (S. L. Suib, and M. E. Davis, Eds.) Vol. 517 p. 383. ACS Symposium Series, 1993.
16. Madon, R. J., and Taylor, W. F., *Adv. Chem. Ser.* **178,** 93 (1979).
17. Flory, P. J., *J. Am. Chem. Soc.* **58,** 1877 (1936).
18. Wilke, C. R., and Chang, P., *AIChE Journal* **1,** 264 (1955).
19. Albal, R. S., Shah, Y. T., Carr, N. L., and Bell, A. T., *Chem. Eng. Sci.* **39,** 905 (1984).
20. Peter, S., and Weinert, M., *Z. Phys. Chem.* **5,** 114 (1955).
21. Carter, J. L., Cusumano, J. A., and Sinfelt, J. H., *J. Catal.* **20,** 233 (1971).
22. Iglesia, E., Soled, S. L., Fiato, R. A., and Via, G. H., *J. Catal.* **143,** 345 (1993).
23. Vanhove, D., Zhuyong, Z., Makambo, L., and Blanchard, M., *Appl. Catal.* **9,** 327 (1984).
24. Lafayatis, D. S., and Foley, H. C., *Chem. Eng. Sci.* **45,** 2567 (1990).
25. Novak, S., and Madon, R. J., *Ind. Eng. Chem. Fundam.* **23,** 274 (1984).